

## DIGITAL TERRAIN MODEL ON VEGETATED AREAS: JOINT USE OF AIRBORNE LIDAR DATA AND OPTICAL IMAGES

Frédéric Bretar<sup>a</sup>, Nesrine Chehata<sup>b</sup>

<sup>a</sup> Institut Géographique National  
2-4 Av. Pasteur 94165 St. Mandé cedex, France  
Email: Frederic.Bretar@ign.fr

<sup>b</sup> Institut EGID - Université Bordeaux 3  
1 Allée Daguin 33607 Pessac  
Email: Nesrine.Chehata@egid.u-bordeaux.fr

**KEY WORDS:** Airborne Lidar, DTM, Vegetation Index, Classification

### ABSTRACT:

Airborne Lidar system provides the Earth's topography as 3D point clouds. Many algorithms have been implemented to sort out the automatic classification problem as well as the Digital Terrain Model generation (DTM). This is mainly due to the various aspects of landscapes within a global survey which can include urban, forested or mountainous areas. This paper is focused on the generation of DTM over rural areas that are composed of open fields and forests. The methodology we propose is based on the joint use of optical images and Lidar data. It aims at adapting the window size of a morphological-based filtering algorithm to the presence of vegetated areas. In this context, Lidar intensity and optical images are combined to generate a Hybrid Normalized Difference Vegetation Index (HNDVI). A vegetation mask is then calculated with HNDVI and Lidar variance information. The window size continuously varies from a predefined minimum distance to an automatically processed upper boundary. We show with conclusive results the potentiality of a full combination of Lidar data and RGB optical images for improving the generation of fine DTMs on rural environments.

### 1 INTRODUCTION

Airborne Lidar systems are nowadays a popular technique to acquire representations of landscapes as 3D point clouds. One of the first process to be applied to raw Lidar data is a classification step, providing ground and off-ground points, and a Digital Terrain Model generation step. These two steps have been a research topic for some years. The generation of DTMs requires efficient algorithms to process large data volumes on various and complex landscapes such as urban areas (Dellcqua et al., 2001), forest areas (Kraus and Pfeifer, 1998) (Haugerud and Harding, 2001) or mountainous areas (Wack and Stelzl, 2005). Many algorithms have been implemented and tested so far, but no generic solution appeared (Sithole and Vosselman, 2003).

Methodologies based on a progressive TIN (Axelsson, 2000) are popular but parameters highly depend on the terrain slope as well as on the relevancy of laser points to belong to the terrain: last pulse is not always a true ground point, especially in presence of dense vegetation coverage. In a DTM production context, the terrain surface as well as the classification result have to be locally and manually corrected.

Methodologies based on a local estimation of the terrain (morphological approaches) suffer from the same drawbacks (Eckstein and Munkelt, 1995) (Kilian et al., 1996). More specifically, the potential of morphological filters to provide a good estimate of the ground depends on the filtering window size and on the distribution of the buildings and trees in the data. If a small window size is used, the local topography will be well represented, provided that there are enough true ground points within the neighborhood. Nevertheless, points belonging to large roof structures will not be filtered as off-ground points. On the contrary, a large window size will tend to over-filter Lidar points and to smooth the final DTM. A solution to overcome these effects is to affine locally the window size of the filter (Kilian et al., 1996) (Zhang et al., 2003).

This study is focused on the generation of DTM over vegetated areas. We propose in this paper a methodology which aims to adapt the window size of a morphological-based filtering algorithm to the presence of vegetated areas (Bretar et al., 2004). In this context, Lidar intensity and optical images are combined

to generate a Hybrid Normalized Difference Vegetation Index (HNDVI). A vegetation mask is then calculated with HNDVI and Lidar variance information. The window size continuously varies from a predefined minimum distance to an automatically processed upper boundary.

After presenting the filtering algorithm, we will describe the generation of the vegetation mask as well as the adaptive window size strategy. Results are finally presented and analyzed.

### 2 BACKGROUND

This part briefly reminds the classification algorithm presented in (Bretar et al., 2004). From an initial location (minimal altitude of the point cloud), the filtering algorithm propagates within the point cloud following the processed region frontier  $\mathcal{F}_{\leq}$ , namely following the steepest local slope over a 4-connexity neighboring system  $\mathbb{V}_s^{4c}$ . Eligible locations evolve within a sorted (ascending order) container structure ( $\mathcal{F}_{\leq}$ ). At each site\*  $s \in \mathcal{F}_{\leq}$ , a square neighborhood  $\mathcal{V}_s$  of dimension  $\mathbf{d}_s$  is extracted.  $\mathbf{d}_s$  is set so that the overlapping ratio between two adjacent locations should be at least of 50%. In the previous work,  $\mathbf{d}_s$  is kept constant for each site  $s$ . At site  $s$ , an initial estimate of the terrain elevation is performed by calculating an average value of laser point height belonging to a rank filtered subset ( $\mathcal{R}_{0.2}(s)$ ). In our case, a ratio of 0.2 has been defined, but it depends on the data quality.

The filtering algorithm is based on a bipartite voting process. Laser points will be classified as **ground** or **off-ground** points depending on their height difference to the local terrain estimate  $|\hat{h}_{\text{ground}}(s) - l_z| < T, T \in \mathbb{R}$ .  $\hat{h}_{\text{ground}}(s)$  is calculated by averaging the altitudes of laser points belonging to  $\mathcal{V}_s$  and classified as **ground**. Considering the overlapping ratio of the neighborhoods, laser points are classified several times either as ground ( $n_s^{\text{ground}}$ ) or off-ground ( $n_s^{\text{offground}}$ ) points.

In order to check the coherence of  $\hat{h}_{\text{ground}}(s)$  with regard to the DTM values over a  $3 \times 3$  window centered in  $s$  ( $DTM^{3 \times 3}(s)$ ), which is a memory of all previously calculated terrain altitudes, we integrate a linear correction to the final value of the DTM at location  $s$ . This correction depends on a coefficient  $\alpha$ , on

\*In image processing, a site corresponds to a pixel (i,j).

$\hat{h}_{\text{ground}}$  and on a mean DTM over a  $3 \times 3$  window centered in  $s$  ( $DTM^{3 \times 3}(s)$ ).

$$DTM(s) = \alpha \hat{h}_{\text{ground}}(s) + (1 - \alpha) \overline{DTM^{3 \times 3}(s)} \quad (1)$$

Finally, for each neighborhood extraction  $\mathcal{V}_s$ , laser points will be labeled following local criteria. At the end of the propagation, a laser point will have been labeled  $n$  times as ground and  $m$  times as non-ground. We then affect the final label corresponding to  $\max(n, m)$ , which is the most representative vote. Algorithm 1 summarizes the algorithm.

---

**Algorithm 1:** Algorithm for classifying laser points

---

**begin**

**Input :**  $\alpha \in [0, 1]$ ,  $T = 0.5\text{m}$

**while**  $\mathcal{F}_{\leq} \neq \emptyset$  **do**

Extraction of  $\mathcal{V}_s$  of dimension  $\mathbf{d}_s$

$\hat{h}_{\text{ground}}(s) = \mathcal{R}_{0.2}(s)$

**foreach** laser point  $l \in \mathcal{V}_s$  **do**

**if**  $|\hat{h}_{\text{ground}}(s) - l_z| < T$  **then**

$l \in \text{ground}; ++n_s^{\text{ground}}$

**else**  $l \in \text{off-ground}; ++n_s^{\text{offground}}$

$\hat{h}_{\text{ground}}(s) = \text{mean}(l_z / l \in \text{ground})$

$DTM(s) = \alpha \hat{h}_{\text{ground}}(s) + (1 - \alpha) \overline{DTM^{3 \times 3}(s)}$

$\mathcal{F}_{\leq} = \mathcal{F}_{\leq} \setminus \{s\}$

$\mathcal{F}_{\leq} = \mathcal{F}_{\leq} \cup \mathbb{V}_s^{4c}$

**end**

---

### 3 METHODOLOGY

#### 3.1 Predicting vegetated areas

This part is dedicated to the generation of a high vegetation mask including hedges, isolated trees and forest areas, but agricultural fields. It is a prediction of vegetated areas based on both the analysis of images and Lidar data.

Typical vegetation has higher reflectance in the near-infrared wavelengths (700-1350 nm) than in the visible domain because red light is mostly absorbed by the plant's chlorophyll (90%). The contrast in reflectance between the red and the near-infrared makes possible to create an image that separates vegetated land cover from non-vegetated land cover by calculating the Normalized Difference Vegetation Index. As usual in a Lidar survey, Lidar data are very often combined with a RGB image acquisition, but infrared channel is not always available, such is the case in this study. We therefore decided to investigate the potential of Lidar intensity information as infrared channel.

Recorded intensity is a function of many variables such as laser power, target reflectivity, range, incidence angle, media absorption (Coren et al., 2005). It also depends on the detection mode applied in the first/last pulse systems (Wagner et al., 2004). The intensity values need to be better calibrated by system developers (Ahokas et al., 2006) or at least to be corrected by scanning homogeneous targets to compute and validate a backscattering model (Coren and Sterzai, 2006). However, if these assumptions are particularly relevant, we decided to investigate the potential of using raw uncalibrated Lidar intensity in case of a joint index computation, which is generally derived from image-based infrared data.

Lidar intensities are therefore resampled at a resolution which depends on the point density. The resampled intensity is calculated on a regular grid by extracting a circular neighborhood of 2.5 m diameter. This choice ensures that enough Lidar points belong to the neighborhood. The final intensity value is the mean

of the intensities of 3D Lidar points included in this neighborhood (with a point density of 0.7 pt/m<sup>2</sup> there are  $\sim 14$  Lidar points). The dynamic of raw intensity values is low with very few saturated values (out of the main distribution). Seeing that the orthophoto is an 8-byte image, the main distribution of intensity values is stretched between 0 and 255. An Hybrid-NDVI is then calculated by:

$$\text{HNDVI} = \frac{\mathcal{I}_{\text{Lidar}} - R}{\mathcal{I}_{\text{Lidar}} + R} \quad (2)$$

where  $R$  is the red channel of the optical image and  $\mathcal{I}_{\text{Lidar}}$  is the Lidar intensity image.

Vegetation is detected by thresholding the HNDVI image. According to (Lillesand and Kiefer, 1994), the values of NDVI for vegetation range is from a low 0.05 to a high 0.66. Applied to our Hybrid-NDVI, these thresholds provided fairly good results.

In order to segregate high vegetation from fields, we crossed this threshold with a binary standard deviation mask: only sites  $s$  such as  $\sigma(s)$  greater than 1 m are considered. Finally, the vegetation mask is defined as a set  $\mathcal{M}$  defined as:

$$\mathcal{M} = \left\{ s / \text{HNDVI}(s) \in [0.05, 0.66] \cap \sigma(s) \geq 1 \text{ m} \right\} \quad (3)$$

and is represented as an image of the same resolution as both the orthophoto and the DTM's one. Figure 1(b) illustrates a vegetation mask calculated for this study.

#### 3.2 Adapting the local neighboring system

As mentioned in the introducing part, the window size of the neighboring system  $\mathbf{d}_s$  (defined in section 2) in case of a morphological-based classification process should be small enough to keep all ground details but large enough to ensure the removal of up-ground objects such as trees or/and buildings. The section describes an algorithm for adapting the window size  $\mathbf{d}_s$  of the structural element ( $\mathcal{V}_s$  is a square window) at site  $s$  to vegetated areas. The adaptative window size  $\mathbf{d}_s$  is processed over laser points belonging to mask  $\mathcal{M}$ . By definition, if a laser point is included into  $\mathcal{M}$ , it is likely to belong to a vegetated area.  $\mathbf{d}_s \in [\mathbf{d}_s^{\min}, \mathbf{d}_s^{\max}]$  should therefore be enlarged to ensure that enough laser points within  $\mathcal{V}_s$  belong to the true terrain.

$\mathbf{d}_s^{\min}$  is a critical parameter and has to be defined so that a minimum number of laser points should be processed within  $\mathcal{V}_s$ . Besides,  $\mathbf{d}_s^{\min}$  ensures the overlapping structure of neighborhoods. We therefore constrain  $\mathbf{d}_s$  as:

$$\mathbf{d}_{\min}^{\text{abs}} < \mathbf{d}_s^{\min} \leq \mathbf{d}_s \leq \mathbf{d}_s^{\max} \quad (4)$$

where  $\mathbf{d}_{\min}^{\text{abs}}$  is a global minimal window size over the entire survey and is independent on site  $s$ . If  $p$  (0.2 in this paper as mentioned previously) is the percentage of lowest laser points within  $\mathcal{V}_s$ ,  $r$  the DTM ground resolution and  $\bar{\delta}$  the global average point density,  $\mathbf{d}_{\min}^{\text{abs}}$  is defined as:

$$\mathbf{d}_{\min}^{\text{abs}} = \max\left(\frac{1}{p * \bar{\delta}}, r\right) \quad (5)$$

In our algorithm,  $\mathbf{d}_s^{\min}$  depends on two parameters: i) the local standard deviation  $\sigma_s^{\text{local}}$  calculated on the  $p\%$  lowest laser points of  $\mathcal{V}_s$  and ii) the neighboring laser points that belong to  $\mathcal{M}$ . The higher the local standard deviation  $\sigma_s^{\text{local}}$ , the larger the minimum window size  $\mathbf{d}_s^{\min}$ . Statistically, low standard deviations of altitudes are over represented in rural areas. Therefore,  $\mathbf{d}_s^{\min}$  has to be highly increasing with low values of  $\sigma_s^{\text{local}}$ . We then define the variations of  $\mathbf{d}_s^{\min}$  as:

$$\mathbf{d}_s^{\min} = \mathbf{d}_{\min}^{\text{abs}} + K \log(1 + \sigma_s^{\text{local}}) \quad K \in \mathbb{R} \quad (6)$$

$K = 6$  was found to be a good compromise for processing our data. To ensure the regularity of adjacent  $\mathbf{d}_s^{\min}$  values, a Gaussian



(a) 2.5 m-Orthoimage.



(b) 2.5 m-Vegetation mask (white pixels) superimposed on the orthoimage.

Figure 1: Generation of a vegetation mask using Lidar data and optical images.

filter is applied over the  $\mathbf{d}_s^{\min}$  image providing that equation 4 is still satisfied.

$\mathbf{d}_s^{\min}$  also depends on the neighboring laser points that belong to  $\mathcal{M}$ . This criteria discriminates small vegetated regions from forests. From an initial value calculated in equation 6,  $\mathbf{d}_s^{\min}$  is increased by one DTM's resolution unit until there is at least one cell of mask  $\mathcal{M}$  that is not considered as a vegetation point.

$\mathbf{d}_s^{\max}$  is set proportional to  $\mathbf{d}_s^{\min}$ . A low value of  $\mathbf{d}_s^{\min}$  should correspond to a small vegetated area and  $\mathbf{d}$  has therefore to vary in a small interval. On the contrary, a high  $\mathbf{d}_s^{\min}$  is likely to correspond to a forest area. To ensure terrain points be statistically represented in  $\mathcal{V}_s$ ,  $\mathbf{d}$  has to vary within a large interval. In this study, we set  $\mathbf{d}_s^{\max} = 3\mathbf{d}_s^{\min}$ .

For each site  $s$  and a window size of  $\mathbf{d}_s^{\min}$ , let us consider the percentage of predicted vegetation area in  $\mathcal{V}_s$  :

$$x_s = \frac{\text{Vegetated surface of } \mathcal{V}_s}{\mathbf{d}_s^{\min} * \mathbf{d}_s^{\min}} \in [0, 1] \quad (7)$$

The behavior of  $\mathbf{d}_s$  between  $\mathbf{d}_s^{\min}$  and  $\mathbf{d}_s^{\max}$  is not a linear function because the window size has to be strongly enlarged in case of a high vegetated ratio where lowest points are not guaranteed to belong to the true terrain. Meanwhile, in case of low ratios, one can expect that lowest laser points belong to the true terrain and describe it in details.  $\mathbf{d}_s$  will consequently increase exponentially with  $x_s$  following equation 8.

$$\mathbf{d}_s(x_s) = A e^{\beta x_s^2} + B \quad (8)$$

With

$$\begin{cases} \mathbf{d}_s(0) = \mathbf{d}_s^{\min} \\ \mathbf{d}_s(1) = \mathbf{d}_s^{\max} \end{cases}$$

we have

$$A = \frac{\mathbf{d}_s^{\max} - \mathbf{d}_s^{\min}}{e^{\beta} - 1} \text{ and } B = \mathbf{d}_s^{\min} - A$$

Parameters in equation 8 were chosen so that  $\mathbf{d}_s$  should be highly enlarged when more than half the structural element size contains dense vegetation, i.e. when  $x_s > 0.5$ . We therefore choose a  $x_s^2$  dependency of the exponential function and  $\beta = 3$  for two main grounds (figures 2 and 3):

- i. the slope is smaller than a simple exponential when  $x_s < 0.5$ . This ensures a regularized  $\mathbf{d}_s$  map that is not sensitive to low vegetated areas.
- ii. the slope is higher than a simple exponential when  $x_s > 0.5$ . This ensures a quick increase of the window size in case of dense vegetated areas.

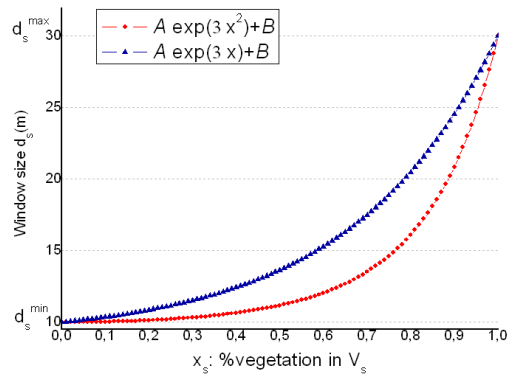


Figure 2: Comparison of two parametric forms of  $d_s$ .

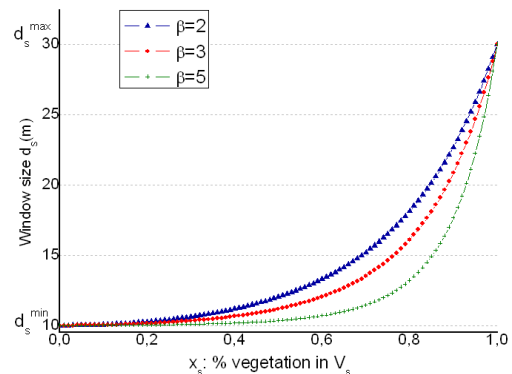


Figure 3: Variations of  $d_s$  with  $\beta \in \{2, 3, 5\}$ .

#### 4 THE DATA SET

Lidar data have been collected in 2004 by the Institut Français de Recherche pour l'Exploitation de la Mer (IFREMER) over the Morbihan's Gulf, France. It has been funded by the foundation TOTAL. The entire survey is composed of 230.10<sup>6</sup> points with

intensities and has been acquired with an ALTM (Optech) system 1210. The point density is  $0.7 \text{ pt/m}^2$ . The Lidar wavelength is 1064 nm.

Optical images are extracted from the BDOrtho® (French orthophoto data basis) of the Institut Géographique National (IGN) with a nominal resolution of 0.5 m, but resampled at 2.5 m for the generation of the Hybrid-NDVI image.

## 5 RESULTS AND DISCUSSION

This part describes the results of the algorithm as well as the impact of the joint use of Lidar data and RGB images on the generation of fine DTMs on vegetated areas. The algorithm has been tested on a large data set described above. We present the results obtained from two  $2\text{km} \times 2\text{km}$  square subset of the Morbihan's Gulf called *GM-7-5* and *GM-6-5* in figure 7.

DTMs presented in Figures 7(a) and 7(e) have been calculated with a constant  $\mathbf{d}_s = 10 \text{ m}$  with solely 3D Lidar data. We clearly observe that such value of  $\mathbf{d}_s$  is well adapted to the retrieval of the terrain over open field areas with a high level of details (field delineations, roads). However, when comparing figure 7(a) with the corresponding aerial image in figure 1(a), one can notice that forested areas are mis-classified providing an erroneous estimate of the DTM over these areas as expected. It is also visible on both profiles presented in figures 4 top and 5 top where grey curves represent the DTM calculated with a constant window size. When increasing the structural element size  $\mathbf{d}_s$  up to 30 m (figures 7(b) and 7(f)), most of vegetated areas have been filtered off. But, many details were lost during this process, providing a smooth DTM.

Figures 7(c) and 7(g) show two DTM calculated with the adaptive window size strategy using 3D Lidar data, Lidar intensity and RGB optical image. Both of them have been post-processed by a Markovian regularization (Bretar, 2007). This post-process consists of minimizing an energy in a Bayesian context. This energy is composed of a data term and a regularization term. The first one describes the Euclidian distance between the surface (the DTM) and the Lidar points classified as terrain points. The second one aims to compensate the effect of the data term so that the final surface should not be too noisy. This term depends on the intrinsic geometry of the surface. We define the regularization term  $\mathcal{E}_r$  as a function of the trace and the determinant of the Hessian matrix  $\mathbf{H}$ .

$$\mathcal{E}_r = \alpha_1 \text{tr}(\mathbf{H})^2 - \alpha_2 \det(\mathbf{H}) \quad (9)$$

with  $\alpha_2 \geq 0$  and  $\alpha_1 \geq \frac{\alpha_2}{2}$

The trace describes the local convexity of the surface while the determinant is linked to the shape of the surface with regard to its tangent plane (parabolic, elliptic, hyperbolic). A steepest gradient algorithm has been used to solve the optimization problem.

One can observe that microrelieves calculated with a constant  $\mathbf{d}_s = 10 \text{ m}$  are preserved while terrain points are better estimated under vegetated areas. The calculated DTM shows interesting meso-relieves such as shallow valleys covered by dense vegetation. It is a cross validation of our algorithm since no exhaustive field campaign have been performed so far.

Figure 7(d) shows the related distance image based on the Hybrid-NDVI mask (see section 3.2). Inverse grey levels are related to distance values included in  $[5\text{m}, 130\text{m}]$ . Darker pixels correspond to large structural elements and are linked to vegetated areas, while brighter pixels correspond to open fields. When looking closely to the image of distances, one can observe the strip-like parallel pattern of the Lidar acquisition survey. The higher point density of overlapped areas are visible as slightly darker vertical strips on figure 7(d). This effect can be explained by the definition of  $\mathbf{d}_{\min}^{\text{abs}}$  in equation 5 where the density is taken into account.

We show on figures 4, 5 and 6 three relevant profiles where Lidar points are plotted along a transect of  $\sim 2\text{km}$ . The final terrain elevation values are plotted as a back lines. The secondary plots represent the corresponding adaptive window sizes along the profile. These curves show that the structural element of the filter evolves depending on the complexity of the off-ground topography and is well-adapted to the estimations of the terrain elevation. Sometimes, when the window size is the largest, the terrain can be over-estimated since it results from the averaging of minimal elevations.

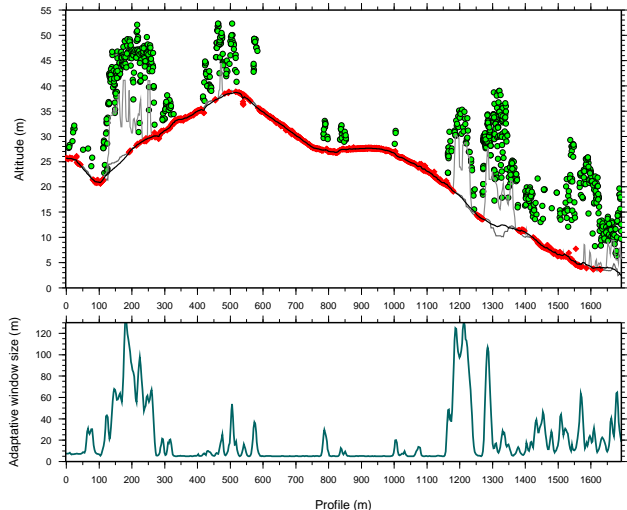


Figure 4: **Top:** Profiles (*GM-7-5*) of classified Lidar points (green  $\rightarrow$  off-ground, red  $\rightarrow$  ground). Grey lines are computed with a constant  $\mathbf{d}_s = 10 \text{ m}$  and  $\mathbf{d}_s = 30 \text{ m}$ . The final terrain is represented as a black line. **Down:** Adaptive window sizes corresponding to the profile.

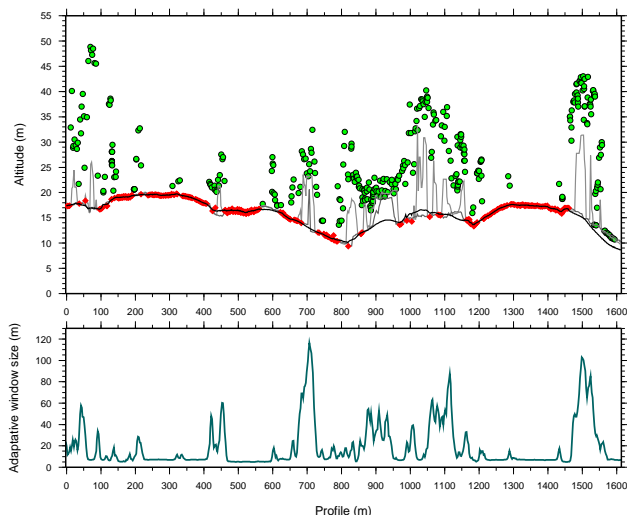


Figure 5: **Top:** Profiles (*GM-7-5*) of classified Lidar points (green  $\rightarrow$  off-ground, red  $\rightarrow$  ground). Grey lines are computed with a constant  $\mathbf{d}_s = 10 \text{ m}$  and  $\mathbf{d}_s = 30 \text{ m}$ . The final terrain is represented as a black line. **Down:** Adaptive window sizes corresponding to the profile.

In this study, we have not given any physical interpretation of Lidar intensity. The distribution of the Lidar intensity image has been artificially stretched for coherence purpose with regard to the orthophoto red channel. As future work, we plan to compare optical infrared channel with Lidar intensity in order to give more physical content of the Lidar intensity image as well as to calibrate both infrared sources.

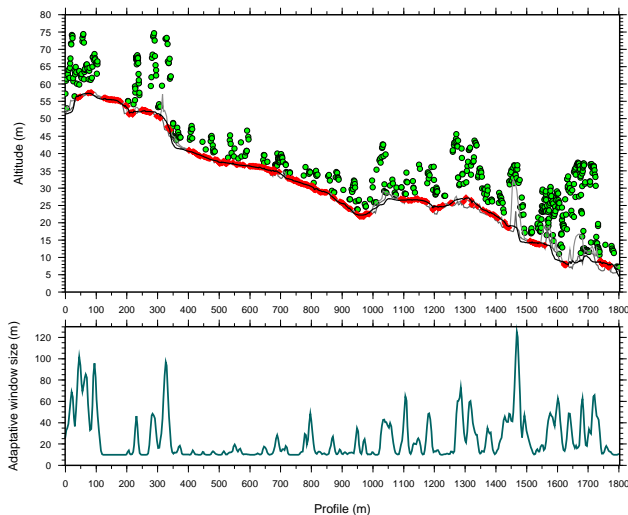


Figure 6: **Top:** Profiles (GM-6-5) of classified Lidar points (green→ off-ground, red→ ground). Grey lines are computed with a constant  $d_s = 10$  m and  $d_s = 30$  m. The final terrain is represented as a black line. **Down:** Adaptive window sizes corresponding to the profile.

The vegetation mask results from the coarse thresholding of the Hybrid-NDVI image (equation 3). The vegetation areas may be punctually under-detected leading to non-dense vegetated regions (figure 1(b)). Indeed, the Lidar survey and the aerial optical images have not been acquired at the same time. Moreover, Lidar intensity is not as reliable as an optical infrared channel. Nevertheless, the overlapping constraint as well as the regularity of the window size of adjacent  $\mathcal{V}_s$  ensure that under-detected vegetation areas are treated as they were. Therefore, there is no need to process a finer vegetation mask.

## 6 CONCLUSION

The paper presents a full methodology for using jointly 3D Lidar data, Lidar intensity and RGB images within the context of DTM generation on vegetated areas. We showed that mixing Lidar intensity values together with RGB optical images in an Hybrid Normalized Vegetation Index is a promising approach for processing rural landscapes with open fields and high vegetation even if both data sets have not been acquired simultaneously. Besides, we showed that, in a typical acquisition framework of RGB images with Lidar data (point cloud and intensity), it is possible to highly improve the classification process for generating a fine DTM.

## REFERENCES

- Ahokas, E., Kaasalainen, S., Hyypä, J. and Suomalainen, J., 2006. Calibration of the Optech ALTM 3100 laser scanner intensity data using brightness targets. In: Proc. of the ISPRS Commission I Symposium, IAPRS, Marne-la-Vallee, France.
- Axelsson, P., 2000. Dem generation from laser scanner data using adaptive tin models. IAPRS, Vol. XXXIII part B4/1, pp. 110–117.
- Bretar, F., 2007. Processing fine digital terrain models by markovian regularization from 3D airborne lidar data. In: ICIP 2007, IEEE, San-antonio, Texas.
- Bretar, F., Chesnier, M., Pierrot-Deseilligny, M. and Roux, M., 2004. Terrain modeling and airborne laser data classification using multiple pass filtering. In: Proc. of the XXth ISPRS Congress, IAPRS, Vol. XXXV part B, ISPRS, Istanbul, Turkey, pp. 314–319.
- Coren, F. and Sterzai, P., 2006. Radiometric correction in

laser scanning. International Journal of Remote Sensing 27(15), pp. 3097–3104.

Coren, F., Visintini, D., G., P. and Sterzai, P., 2005. Integrating lidar intensity measures and hyperspectral data for extracting of cultural heritage. In: Proc. of Workshop Italy-Canada for 3D Digital Imaging and Modeling: applications of heritage, industry, medicine and land.

Dellcqua, F., Gamba, P. and Mainardi, A., 2001. Digital terrain models in dense urban areas. In: Proc. of the ISPRS Workshop on land surface mapping and characterization using laser altimetry, IAPRS, Vol. XXXIV-3/W4, Annapolis, U.S., pp. 195–202.

Eckstein, W. and Munkelt, O., 1995. Extracting objects from digital terrain models. In: Proc. Int. Society for Optical Engineering: Remote Sensing and Reconstruction for Three-Dimensional Objects and Scenes, Vol. 2572, pp. 43–51.

Haugerud, R. and Harding, D., 2001. Some algorithms for virtual deforestation of lidar topographic survey data. In: Proc. of the ISPRS Workshop on land surface mapping and characterization using laser altimetry, IAPRS, Vol. XXXIV, Annapolis, U.S., pp. 211–218.

Kilian, J., Haala, N. and Englich, M., 1996. Capture and evaluation of airborne laser scanner data. IAPRS, Vol. XXXI, pp. 383–388.

Kraus, K. and Pfeifer, N., 1998. Determination of terrain models in wooded areas with airborne laser scanner data. ISPRS Journal of Photogrammetry and Remote Sensing 53, pp. 193–203.

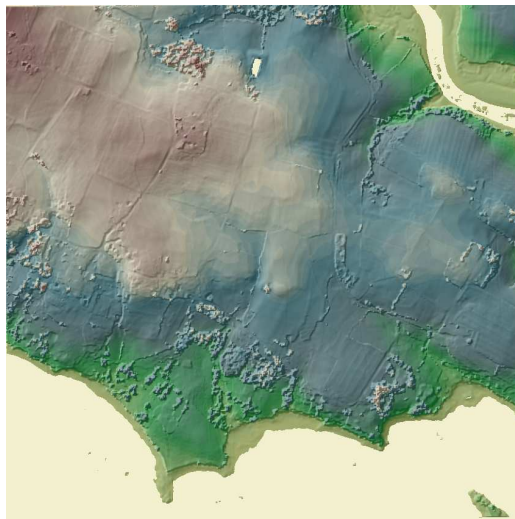
Lillesand, T. and Kiefer, R., 1994. Remote Sensing and Image interpretation. John Wiley & Sons.

Sithole, G. and Vosselman, G., 2003. Comparison of filtering algorithms. In: Proc. of the ISPRS Workshop III/3 '3D Reconstruction from Airborne Laserscanner and InSAR', IAPRS, Vol. XXXIV, Dresden, Germany, pp. 71–78.

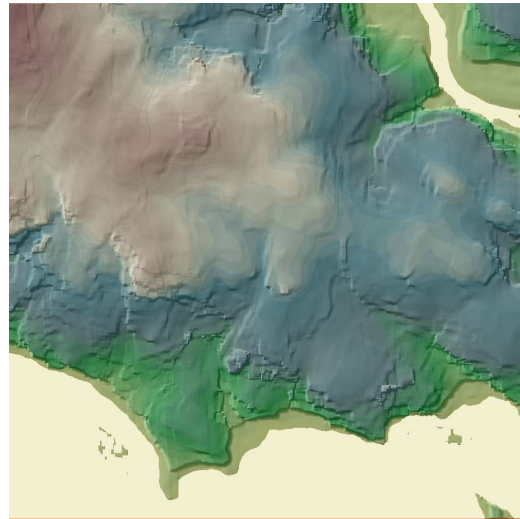
Wack, R. and Stelzl, H., 2005. Laser DTM generation for South-Tyrol and 3D-visualization. In: Proc. of the ISPRS Laserscanning 2005, IAPRS, Vol. XXXVI-3/W19, Enschede, the Netherlands, pp. 48–53.

Wagner, W., Ullrich, A., Melzer, T., Briese, C. and Kraus, K., 2004. From single-pulse to full-waveform airborne laser scanners: Potential and practical challenges. IAPRS, Vol. 35, Part B3, pp. 201–206.

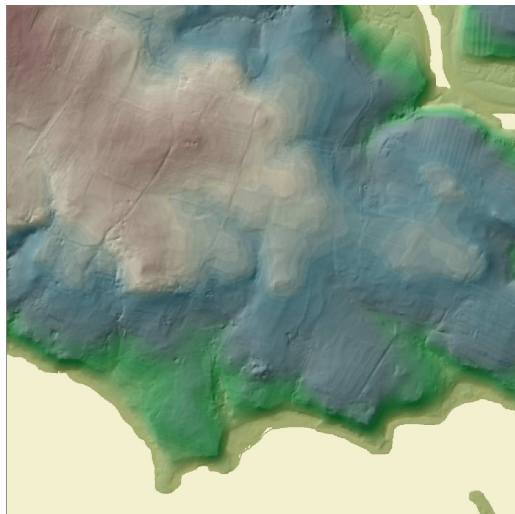
Zhang, K., Chen, S.-C., Whitman, D., Shyu, M., Yan, J. and Zhang, C., 2003. A progressive morphological filter for removing nonground measurements from airborne lidar data. IEEE Transactions on Geoscience and Remote Sensing 41(4), pp. 872–882.



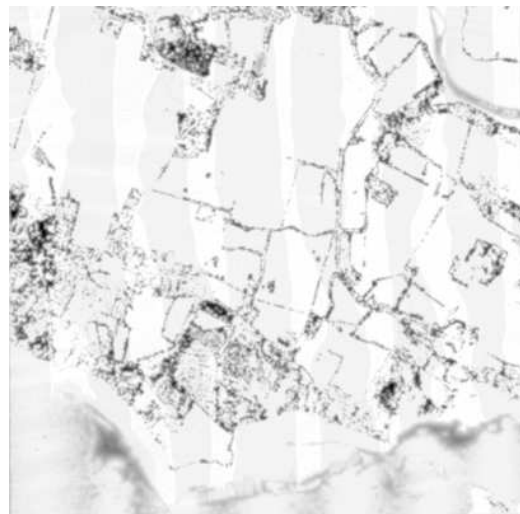
(a) DTM from Lidar data with  $d_s = 10$  m.



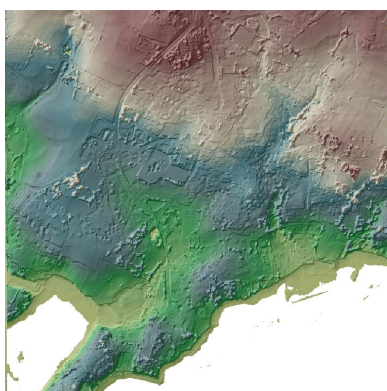
(b) DTM from Lidar data with  $d_s = 30$  m.



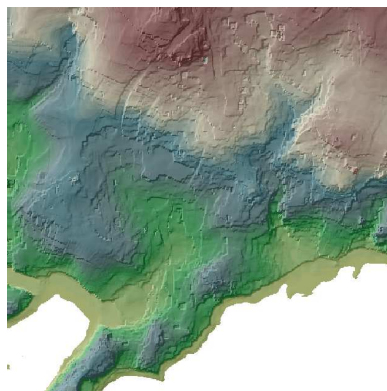
(c) DTM from Lidar data and RGB images with adaptive  $d_s$ .



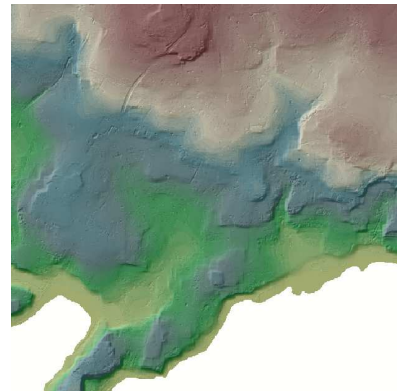
(d) Image  $d_s$  coded in inverse grey level scale.



(e) DTM from Lidar data with  $d_s = 10$  m.



(f) DTM from Lidar data with  $d_s = 30$  m.



(g) DTM from Lidar data and RGB images with adaptive  $d_s$ .

Figure 7: Results of DTM processing over the area GM-7-5 (figures a, b, c, d) and GM-6-5 (figures e, f, g).